BRNO UNIVERSITY OF TECHNOLOGY

FACULTY OF ELECTRICAL ENGINEERING AND COMMUNICATION

Department of Biomedical Engineering

SIMULTANNEOUS EEG-FMRI DATA FUSION WITH GENERALIZED SPECTRAL PATTERNS

FÚZE SIMULTÁNNÍCH EEG-FMRI DAT ZA POMOCI ZOBECNĚNÝCH SPEKTRÁLNÍCH VZORCŮ

Doctoral Thesis - Short version

Ing. René Labounek

Specialization:	Biomedical Engineering & Neurosciences
Academic Advisor:	prof. Ing. Jiří Jan, CSc.
Expert Advisors:	Ing. Michal Mikl, Ph.D.
	David A Bridwell, Ph.D.

Brno, 2018

KEYWORDS

simultaneous EEG-fMRI, heuristic approach, spatiospectral group-ICA, independent component analysis, general linear model, GLM, visual oddball, semantic decision, resting-state, k-means clustering, ICASSO, GIFT, SPM12, EEG Regressor Builder

KLÍČOVÁ SLOVA

simultánní EEG-fMRI, heuristický přístup, prostorovofrekvenční skupinová-ICA, analýza nezávislých komponent, obecný lineární model, GLM, vizuální oddball, semantické rozhodování, resting-state, k-means shlukování, ICASSO, GIFT, SPM12, EEG Regressor Builder

The doctoral thesis is deposited in the Department of Science and Research, Faculty of Electrical Engineering and Communication, Brno University of Technology, Technická 12, 616 00 Brno.

ISBN 80-214-XXXXX
ISSN 1213-418X

CURRICULUM VITÆ

Name: **Ing. René Labounek**
Born: 28. 7. 1988 in Olomouc
Address: Na Výsluní 16, 796 03 Prostějov
E-mail: rene.labounek@gmail.com

Experiences

2017 –	Biomedical Engineer, Department of Biomedical Engineering, University Hospital Olomouc, CZE
2016 –	Research Assistant, Department of Neurology, Palacky University Olomouc, CZE
2015 – 2015	Research Scholar, Center for Magnetic Resonance Research, University of Minnesota, Minneapolis, USA
2012 – 2016	External Co-Worker, CEITEC, Masaryk University, Brno, CZE
2012 – 2014	Research Assistant, Deparmtent of Biomedical Engineering, Brno University of Technology, CZE

Education

2007 – 2012	Biomedical Engineering and Bioinformatics, Faculty of Electrical Engineering and Communication, Brno University of Technology
1999 – 2007	Gymnázium Jiřího Wolkera v Prostějově

Projects & Awards

2016 – 2017	Brain wakefulness detection Open access acquisition time of scalp 256-electrode EEG data
2016	Czech-Bioimaging Open access acquisition time of spinal cord HARDI dMRI data
2015	Joseph Fourier Price Scientific price in computer science awarded by French embassy
2014 – 2016	Advanced analysis of medical and biological systems, signals and data (BUT FEEC Grant)
2012 – 2013	Optimization of methods and evaluations of simultaneous EEG-fMRI (GAP304/11/1318 2012-13)

Teaching

I was teaching laboratories for subjects Analysis of Biomedical Images, Computers and Programming in Czech or English language, and supervised four Bachelor and five Master Theses.

CONTENTS

1 INTRODUCTION **5**

2 DOCTORAL THESIS OBJECTIVES **8**

3 GENERALIZED EEG-FMRI SPECTRAL HEURISTIC MODEL **8**
3.1 Visual oddball task and EEG-fMRI acquisition 8
3.2 Semantic decision task and EEG-fMRI acquisition 9
3.3 EEG and fMRI data preprocessing 10
3.4 EEG regressor deviations for the distinct frequency bands 10
3.5 Experiments with visual oddball EEG data 11
3.6 Joint EEG-fMRI analysis 11
3.7 Assesment of group-averaged EEG-fMRI SPMs 11
3.8 Assesment of task-related variability in EEG regressors 12
3.9 Results 12
3.10 Conclusion 15

4 EEG-FMRI SPATIOSPECTRAL HEURISTIC MODEL **16**
4.1 Visual oddball and semantic decision datasets 16
4.2 Resting-state paradigm and EEG-fMRI acquisition 16
4.3 EEG and fMRI data preprocessing 16
4.4 EEG spatiospectral decomposition 16
4.5 Clustering of spatiospectral maps across paradigms 17
4.6 Spatiospectral pattern dynamics and stimuli vectors 18
4.7 EEG-fMRI GLM with variable HRFs 18
4.8 Results 18
4.9 Novelty in EEG decomposition and following EEG-fMRI fusion . . . 23
4.10 Conclusion 24

5 DOCTORAL THESIS OUTCOMES AND CONCLUSIONS **24**

6 ABSTRACT **27**

1 Introduction

Since Isidor Rabi (1937) declared and measured atom's nuclear magnetic resonance at molecular beams [40], Felix Bloch and Edward Purcell (1946) expanded it at liquid and solid measurements [4, 39] and Paul Lauterbur (1973) introduced basal principles of magnetic resonance imaging (MRI) [32], many different MRI sequences able to visualize different chemico-physical phenomena were invented. In biomedical imaging applications, different chemico-physical image contrasts can provide different qualitative and quantitative information about in-vivo displayed tissue. After 1990, Ogawa's et al. MRI sequences sensitive to blood oxygenation (BOLD signal) [37] gave raise to the field called functional magnetic resonance imaging (fMRI) because repetitive time of one 3D image scanning fulfills the Nyquist theorem for capturing of dynamic cardio-vascular changes evoked by induced neuronal activity.

Practically immediately after BOLD signal discovery (blood oxygen level dependence) [37], other scientists started to think about simultaneous recording of scalp electrophysiological and functional MRI data. They solved it between 1993-1995 and scientific field called simultaneous EEG-fMRI was born [18]. Allen et al. and Goldman et al. suppressed gradient artifacts from scalp EEG signals with cumulative signal filtering techniques [2, 15] and the fusion of simultaneous EEG-fMRI data has become to be possible[16, 31].

In simultaneous EEG-fMRI, we are trying to explain the measured delayed BOLD signal $\boldsymbol{b}$ with immediate EEG signal changes transformed into some latent form $\boldsymbol{e}$ (eq. 1). The impulse response function (IRF) $\boldsymbol{h}$ models the BOLD signal's delay. The motivation is to be able to visualize the functionally relevant brain network without a-prior knowledge of the stimulus timings as a blind search data-driven analysis.

$$\boldsymbol{b} = \boldsymbol{e} * \boldsymbol{h} \tag{1}$$

The fixed canonical hemodynamic response function (HRF) is the most often used IRF for the BOLD signal delay modelling [29]. However, linear combinations of hemodynamic response basis functions better accounts for differences in HRF shape and timings across subjects and brain areas [35]. Alternatively, HRF may be estimated in a data-driven manner by deconvolution of the EEG and fMRI time courses [8].

Beside the question of the IRF's proportions, the EEG signal processing into $\boldsymbol{e}$ form (eq. 1) becomes much more fundamental problem because we need to fulfil two basic conditions:

1. Transform the raw EEG signal onto comparable form with the BOLD signal.
2. Still keep the advantage of better EEG's temporal resolution inside a transformed signal, although it was down-sampled onto fMRI timings.

Previously most often used transformations of raw EEG signal to the latent $\boldsymbol{e}$ form can be divided at two distinct groups. The 1^{st} approach emphasizes the detection of previously defined EEG waveform shapes (i.e. graphoelements), including evoked or

event-related potentials (EPs or ERPs) [3] or epileptic spikes [43]. The 2^{nd} most common approach (which is in the scope of the current thesis) is to integrate EEG spectra with fMRI BOLD signal [8, 12, 16, 23, 28, 29, 30, 31, 33, 34, 35, 41].

Motivation and main goal of the current doctoral thesis is to improve visualization of task-related networks directly and blindly from simultaneous EEG-fMRI data without a-prior knowledge of external stimulation timings. Kilner et al.(2005) proposed a theoretic heuristic approach comparing EEG and BOLD signals on the level of neuronal activity, since their solution (relation 2) expects that changes in BOLD signal b are proportional to neuronal activity a which is proportional to changes in root mean square frequency of whole normalized (relative) EEG power spectrum $p(\omega)$ [23]. The character $\tilde{}$ indicates variables during increased activity, while variables without $\tilde{}$ represent signal values during rest. The normalized (relative) EEG power can be more extensively rewritten with standard spectral density $g(\omega)$ with eq. 3.

$$\left[\frac{\tilde{b}}{b}\right]^2 \propto (1+a)^2 \propto \frac{\int \omega^2 \tilde{p}(\omega) d\omega}{\int \omega^2 p(\omega) d\omega} \tag{2}$$

$$p(\omega) = \frac{g(\omega)}{\int g(\omega) d\omega} \tag{3}$$

Rosa et al. (2010) simplified Kilner's et al. (2005) theoretic heuristic model at relation 4, when they considered the denominators of relation 2 for constant members. The simplified heuristic model was able to visualize the stimulated primary visual cortex from simultaneous EEG-fMRI data better than other standard used approaches utilizing absolute EEG power fluctuations [41].

$$\tilde{b} \propto \sqrt{\int \omega^2 \tilde{p}(\omega) d\omega} \tag{4}$$

It is known that different brain rhythms (frequencies) are dominant for different cognitive states [9]. Although Miller (2010) experimentally measured the broadband spectral changes of local field potentials and their shift to higher frequencies after activations of neural tissue [36], the basic heuristic model (eqs. 2 and 4) [23, 41] neglects the inconsistent changes over different frequencies which are observed e.g. for the EEG α-band rhythm in comparison to the other EEG rhythms [25]. So, we are expecting that it is one of the crucial limitation of the curretn state of the art which is tested within the current doctoral thesis.

The function ω^2 in the expression $\int \omega^2 \tilde{p}(\omega)$ represents the filtering properties emphasizing higher frequencies of the relative EEG power in front of the power of lover frequencies. But if we admit the possibility that some frequencies could behave inconsistently to the others, it means that more possible filtering solutions could exist. And, we are getting from the basic simplified heuristic model (eq. 4) to the generalized spectral heuristic model (eq. 5) (which we have proposed within doctoral thesis [28])

where $g(\omega)$ characterizes a general filtering function (e.g. the α-band or γ-band pass filters.

$$\tilde{b} \propto \sqrt{\int g(\omega)\tilde{p}(\omega)d\omega} \tag{5}$$

Implementation of the generalized spectral heuristic model (eq. 5), obtained results, its advances in front of classic absolute power fluctuations in distinct frequency bands, comparison with classic heuristic model and other evaluations are described within the 3^{nd} *chapter "Generalized EEG-fMRI spectral heuristic model"*, and bring novel knowledges into EEG-fMRI fusion methods.

Although the generalized spectral heuristic model allows more spectral patterns with various dynamic behaviours, it is not still utilizing the advantages of multi-channel recordings. As in case of classic absolute power fluctuations (e.g. [12, 31]), the averaging over selected electrodes of interest is the most often used procedure [41]. But that procedure brings very similar results over different electrode selections as evaluated and described in 3^{rd} *chapter "Generalized EEG-fMRI spectral heuristic model"*.

As shown before, the different EEG oscillations with different spectral properties can have different spatial sources (e.g. [20, 42]). The incorporation of the spatial information into the generalized heuristic model seems to be the other logical step and it can be written as relation 6 characterizing generalized spatiospectral heuristic model (which we introduced [28]).

$$\tilde{b} \propto \sqrt{\int\int g(c,\omega)\tilde{p}(c,\omega)dcd\omega} \tag{6}$$

Within the current doctoral thesis, the estimation of the generalized spatiospectral heuristic model was designed with incorporation of Bridwell's et al. (2013) decomposition [8] on independent EEG spatiospectral patterns. Since the decomposition is a quite novel technique whose stability and relevance has not been tested over set of different datasets yet, the submitted thesis is evaluating that properties for both decompositions (originally used absolute EEG power decomposition, and novelly used relative EEG power decomposition utilizing the spatiospectral heuristic model). Simultaneously, the relevance for the EEG-fMRI data fusion and correspondence of decomposed signals to the external stimulation timings are evaluated and assessed too. As the novel knowledges, all the procedures and obtained results are described in the best details within the 4^{th} *chapter "EEG-fMRI spatiospectral heuristic model"*.

2 Doctoral thesis objectives

As summarized within the Introduction, the process of the full automatic and well-working process of EEG-fMRI data fusion which is single-subject specific is still the not-solved task in the area of the basal research. The main and crucial objective of the current thesis is to try to design and find the optimal EEG-fMRI data processing pipeline which would be able to blindly estimate and visualize the task-related brain networks directly from the captured data, without any prior knowledge about the stimulus timings inside the analysis pipeline. For that final goal, the set of listed partial objectives was designed:

1. Select the EEG signal processing strategy which is usable for the blind search analysis.
2. Design the models for the data fusion which could work better than current state of the art.
3. Design the evaluation and evaluate the correspondence of obtained results with experimental external stimulation.
4. On available real simultaneous EEG-fMRI data, estimate the fusion with designed models, with previously implemented methods and compare the results over the different approaches.
5. Evaluate the designed models and their new contributions to the current knowledge.
6. Present the obtained results in neuroscience or biomedical engineering journals with impact factor as two original research papers (at minimum).
7. Share the implemented software libraries as the doctoral thesis attachment.

To the 1^{st} of the seven partial objectives, we have limited on EEG signal processing methods utilizing the EEG spectra, since a man need to know the stimulus timings for ERP estimations in the most of temporal or spatiotemporal decompositions [3, 6]. It is not necessary for the EEG spectra processing or decomposition.

To the 2^{nd} of the partial objectives, we have designed the generalized spectral and spatiospectral heuristic models (eqs. 5 and 6) [28] which we are testing and comparing with previous methods within the submitted thesis.

3 Generalized EEG-fMRI spectral heuristic model

3.1 Visual oddball task and EEG-fMRI acquisition

A visual oddball task was performed by 22 subjects (7 women; age 23 ± 2 years; 1 left-handed man). Informed consent was obtained from all subjects after all of the procedures were fully explained, and the study received the approval of the local ethics committee. Three stimulus types were presented randomly to each subject. Each stimulus consisted of a single yellow uppercase letter shown for 500 ms on the black background. Inter-stimulus intervals varied from 4 to 6 seconds. A total of 336 stimuli consisted of targets (letter X, 15%), frequents (letter O, 70%) and distractors (letters

other than X and O, 15%). Subjects were instructed to press a button held in their right hand whenever the target stimulus appeared and not to respond to distractor or frequent stimuli. The experiment was divided into four consequential sessions for each person [5, 29].

The imaging was performed by a 1.5 T *Siemens Symphony* scanner equipped with *Numaris 4 System (MRease)*. Functional images were acquired using gradient echo, echo-planar imaging sequence: TR = 1660 ms; TE = 45 ms; FOV = 250 × 250 mm; FA = 80 degrees ; matrix size = 64 × 64 (3.9 × 3.9 mm); slice thickness = 6 mm; 15 transversal slices per scan. The whole task was divided into four equal runs of 256 scans and 84 stimuli. An anatomical T1-weighted high-resolution brain scan (160 sagittal slices, resolution 256 × 256 resampled to 512 × 512, slice thickness = 1.17 mm) was added to the functional data of each subject.

The scalp EEG data, with reference electrode between Cz and Fz electrodes, were acquired simultaneously during the fMRI scanning by a 30-electrode MR compatible EEG system (*BrainProducts, Germany*) with a sampling frequency of 5 kHz [29].

3.2 Semantic decision task and EEG-fMRI acquisition

A semantic decision task was performed by 42 healthy subjects (22 right-handed men, 2 left-handed men, 18 right-handed women; age 25 ± 5 years). Informed consent was obtained from all subjects after all of the procedures were fully explained, and the study received the approval of the local ethics committee. The task was designed with a block stimulation paradigm which elicits robust language network activation [14]. During the probe block, sentences with semantic error created by a phonemic exchange (e.g. The cat was chased by fog) were presented randomly among semantically correct sentences. The sentences were replaced with a series of the X's or O's, (e.g. 'Xxxx xx xxxx xxx.') during the control block. Nine control and eight probe blocks alternated during the experiment. Each block lasted 24s, and consisted of six different control or probe stimuli presented for 3.5s followed by a black screen for 0.5s. Subjects viewed the stimuli through a mirror mounted on the head coil. Responses were not requested from the subjects during the task. After the session, no subjects reported any problems with reading the sentences [27, 35].

The imaging was performed by a 1.5 T *Siemens Symphony* scanner equipped with *Numaris 4 System (MRease)*. High-resolution anatomical T1-weighted MPRAGE images were acquired (160 sagittal slices, matrix size 256 x 256 resampled to 512 x 512, slice thickness = 1.17mm, TR = 1700ms, TE = 3.96ms, FOV = 246mm, FA = 15 degrees). Parameters of fMRI acquisition using gradient echo, echo-planar imaging sequence were: 230 scans, TR = 1850ms, TE = 40ms, FA = 80°, voxel size = 3.9 x 3.9 x 6 mm 3 , no gap between slices, 20 transversal slices. The field of view covered supratentorial regions.

Simultaneously, scalp EEG data were recorded with a 30-electrode MR compatible EEG system (*BrainProducts, Germany*). ECG were recorded to remove physiological

artifacts from EEG. Signals were sampled at 5 kHz with 0.5μV resolution for EEG, and 10μV for ECG [28].

3.3 EEG and fMRI data preprocessing

EEG preprocessing was done using *BrainVision Analyzer 2.0* (*BrainProducts, Germany*) software. The raw EEG data were corrected for the gradient artifacts [1] and down-sampled to 250 Hz. Thereafter, the IIR filter with the pass-band of 1 Hz to 40 Hz was applied. Cardiac artifacts were suppressed by mean artifact subtraction. For the visual oddball EEG data, eye-blinking artifacts were removed using decomposition by temporal ICA [11, 22] and back reconstruction without the eye-blink related component, which were chosen according to specific temporal and spatial topography.

FMRI data were preprocessed in the SPM8 (*Statistical Parametric Mapping version 8, Wellcome Trust Centre for Neuroimaging, UK*). The first preprocessing step was motion artifact minimization, done by aligning all brain scans with registering process utilizing linear rigid geometric transformations [21]. Functional images were co-registered with the high-resolution anatomical image with linear affine geometric transformations [21]. To enable later group studies, the images were normalized to the standardized template of the head in MNI[1] coordinates with non-linear registrations [13] and re-sampled to 3 × 3 × 3 mm isotropic resolution. Images were smoothed by an isotropic spatial filter with a Gaussian profile of FWHM[2] = 8 mm to increase the signal to noise ratio (SNR) and to make the random errors more normally distributed. Finally, the time series of each voxel was filtered to discard the component of the BOLD signal with time periods longer than 128 s which mostly contains slow drifts and physiological noise [29].

3.4 EEG regressor deviations for the distinct frequency bands

EEG regressors were calculated with our EEG Regressor Builder software. Signals measured at the electrodes of interest were selected from the pre-processed EEG data. Each of these signals was segmented onto TR long epochs with corresponding temporal resolution, where TR is the fMRI repetition time. Each EEG signal epoch was transformed into the spectral domain by Discrete Fourier Transform. The frequency band of interest for a given epoch was filtered by zeroing spectral lines outside the band of interest. The absolute or relative power values were calculated from each filtered band for every epoch. The analysed frequency range was from 0 to 40 Hz divided at typical different frequency bands of interest, i.e. $\delta(0-4Hz)$, $\theta(4-8Hz)$, $\alpha(8-12Hz)$, $\beta(12-20Hz)$ and $\gamma(20-40Hz)$.

Temporal power changes were convolved with canonic HRF to respect the similar convolution of the neural events producing the BOLD signals. Only valid samples

[1]Montreal Neurological Institute

[2]Full Width at Half Maximum

without convolution edge effects were used. Convolved vectors were then normalized to mean 0 and variance 1.

3.5 Experiments with visual oddball EEG data

In order to determine the sensitivity of the regressor calculation to the task-related variability with respect to the choice of the above and below mentioned parameters, the EEG regressors were calculated for several types of parameter settings, and the influence on the resulting group statistical parametric EEG-fMRI maps was monitored. The studied parameters were electrodes of interest, frequency bands of interest and types of power values (absolute/relative).

The regressors were calculated for the following parameter combinations: three groups of electrodes (*O1-O2-Oz*, *C3-CP1-CP5* and *all 30 electrodes*), both types of power values (*absolute and relative*), and five frequency bands of interest δ*(0–4 Hz)*, θ*(4–8 Hz)*, α*(8–12 Hz)*, β*(12–20 Hz)* and γ*(20–40 Hz)*. Altogether 30 regressors were calculated for each subject. The selection of electrodes was substantiated as follows: *O1-O2-Oz* electrodes were chosen because primarily the visual cortices were stimulated during the experiment. *C3-CP1-CP5* electrodes are near to the motor cortices which should be activated in reaction to the target stimulus. The global signal power is defined by *all 30 electrodes* [29].

3.6 Joint EEG-fMRI analysis

The derived EEG regressors were compared with single-subject fMRI data within voxel-wise general linear modelling (GLM) separate for each EEG regressor calculation settings. The model matrix contains four EEG regressors from four separate sessions and constant terms in BOLD signals for each session. To preserve task-related variability in the data, regressors describing the stimulation event were not used.

Since 30 EEG regressors were calculated for 22 subjects it means that 660 separate GLM estimations were performed with the SPM8 scripts. For each person, 30 SPMs were estimated. Because the analysis examines only their mutual influence, one SPM represents 3D correlation map between local BOLD signal and EEG regressor with a given parameter setting for corresponding subject.

During the second analytical phase, group analyses were estimated from SPMs of subjects via a one-sample t-test, always using (for the whole group) a particular chosen parameter setting for EEG regressor calculation. The whole analysis output was 30 group-averaged SPMs describing above mentioned correlations.

3.7 Assesment of group-averaged EEG-fMRI SPMs

Different parameter analysis settings (e.g. frequency band, power value,...) can bring different or similar resulting group activation maps. The assessment of similarity of

topology of group activation maps with different parameter sittings was based on joint histogram with 8-bit coding and not-normalized mutual information (MI) [21] between two different 3D activation maps [21, 29].

3.8 Assesment of task-related variability in EEG regressors

The assesment was performed with GLM. EEG regressors for different parameter settings were in data matrix and the model signals in model matrix were the stimulus vectors with convolved canonical HRF. Group analyses across subjects were performed via one sample t-tests separately for each type of stimulation [29].

3.9 Results

Within the current subsection, all mentioned results were obtained only from visual oddball dataset. The semantic decision dataset was not investigated for observing of the same result properties. Figure 1 visualize that different group SPMs are obtained with absolute and relative EEG power regressors with the same setting of other parameters (frequency band of interest, electrode selection). It indicates that relative power provides different information about brain activity than that conveyed by the absolute power [29].

Figure 2 shows that the relative EEG power in different frequency bands of interest correlates with the BOLD signal in different brain areas when other parameters (type of power value, electrode selection) are identical. Relative δ band and relative α band depict similar activation map with 2 differences: positively correlated clusters with BOLD signal for relative δ band are negatively correlated for relative α band and vice versa. Relative α band has higher t-values in SPMs opposite to the relative δ band [29].

Absolute EEG power correlates in very similar way across different frequency bands and contains some broad spectrum component.

MICs in table 1 truly confirm that all three properties observed with visual inspection applies. The EEG-fMRI SPMs of different frequency bands share higher

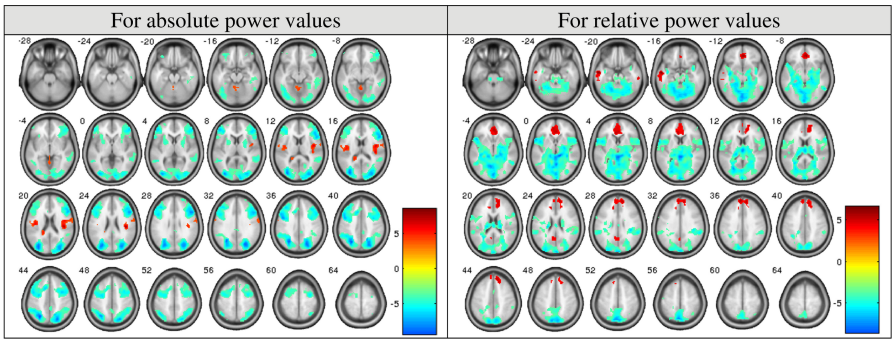

Obrázek 1: Correlations between BOLD signal and EEG power fluctuations in α band for all 30 electrodes of interest (p < 0.001 uncorrected) [29].

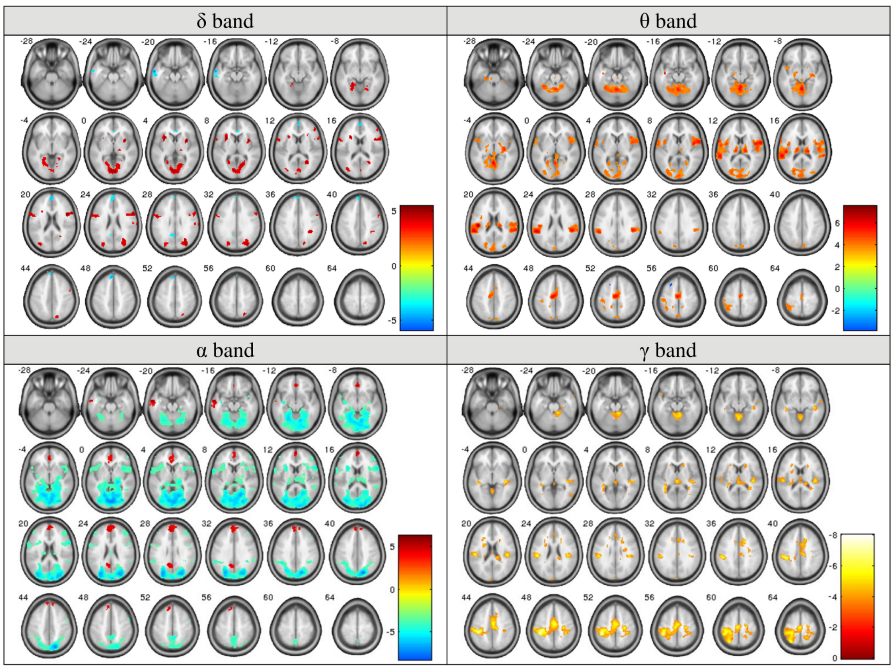

Obrázek 2: Correlations between relative power values of EEG and BOLD signal for δ, θ, α and γ band from O1-O2-Oz electrodes (p < 0.001 uncorrected; for relative β band, statistically significant clusters were not observed) [29].

Tabulka 1: MICs between EEG-fMRI SPMs over different power types and frequency bands: O1-O2-Oz electrodes of interest; On diagonal, there are entropies of given SPMs. Except the diagonal, values higher than 0.75 are highlighted in bold [29].

Absolute power					Relative power						
δ	θ	α	β	γ	δ	θ	α	β	γ		
4.62	**1.15**	0.48	**0.77**	0.70	0.47	0.55	0.49	0.40	0.52	δ	
	4.79	0.52	**0.85**	0.66	0.40	**0.78**	0.49	0.37	0.55	θ	
		4.68	**0.80**	0.69	0.40	0.36	0.49	0.33	0.48	α	Abs. p.
			4.67	**0.82**	0.33	0.43	0.39	0.30	0.56	β	
				4.59	0.32	0.36	0.37	0.33	0.35	γ	
					4.35	0.41	**0.99**	0.38	0.30	δ	
						4.49	0.62	0.30	0.35	θ	
							4.70	0.36	0.33	α	Rel. p.
								4.04	0.30	β	
									4.32	γ	

mutual information for absolute EEG power than for relative EEG power where the values are much lower. Other words, EEG-fMRI SPMs trully differs for relative power over different frequency bands (except relative δ and α bands where the similarity was observed). And finally the third property, all absolute and relative EEG-fMRI SPMs differ mutually, except absolute and relative θ bands.

Visual inspection and MICs (not-shown in short version) confirm, that different selection of electrodes of interest does not affect and does not change the final group-averaged EEG-fMRI results.

Tabulka 2: The relationship between task-related regressors and EEG-derived regressors: The group t-values show effect of each stimulus type on EEG-derived regressors derived from all 30 electrodes. The significance level set to p < 0.05 uncorrected. Significant t-values are highlighted in bold [29].

Stimulus	Absolute power					Relative power				
	δ	θ	α	β	γ	δ	θ	α	β	γ
Target	**3.89**	**5.25**	1.81	**2.84**	0.76	**3.07**	**4.76**	**-5.13**	**-2.69**	**-4.79**
Frequent	1.10	0.54	0.14	0.42	-0.88	**2.09**	-0.26	**-2.12**	-0.65	**-2.69**
Distractor	1.42	1.59	-0.47	0.61	-0.42	**2.09**	1.99	**-4.01**	-0.56	**-3.02**

The GLM between EEG regressors and stimulus vectors with following group-averaging t-test indicates that relative EEG power consist more task-related variability than absolute EEG power (table 2). That means that heuristic approaches should be more usable for visualization of task-related networks from EEG-fMRI data than absolute EEG power fluctuations. Since classic heuristic model (eq. 4) [23, 41] assume only one possible solution in relative EEG power filtration and since we have found heterogeneous EEG-fMRI SPMs for different frequency bands of relative EEG power, generalized spectral heuristic model (eq. 5) could be more accurate for task-related network visualizations.

Visual inspection and MICs were used for evaluations of similarities and differences between EEG-fMRI SPMs estimated with classic heuristic model or with some frequency band of interest of relative EEG power (i.e. generalized spectral heuristic model [28]). The assessment was performed on both datasets (visual oddball and semantic decision tasks).

The EEG-fMRI SPM for classic heuristic model (eq. 4) on visual oddball dataset and seems to be the most similar to the result of relative γ band (Fig. 2). Such observation is consistent with the fact, that both filters reach maximal gain in the same frequency range 20-40Hz. Activated supra-thresholded sensory-motor cortices are truly contralateral to the right-handed pushed button on target stimuli [28]. That brain network can be considered as task-related based on relative γ band results (Tab. 2 and Fig. 2). Mutual information coefficients (Tab. 3) confirm the conclusion that the classic heuristic model result is the most similar to the relative γ band result.

Except sensory-motor network, relative δ and α band patterns demonstrate task-related visual network to be activated (Fig. 2 and Tab. 2). Classic heuristic model is insensitive to that network. Other words based on visual oddball data results, the generalized spectral heuristic model is able to visualize more task-related networks than classic heuristic model. The matrix of MICs over freqquency bands and heuristic model for semantic decision data (shown in full.length thesis) has same properties as the same matrix for visual oddball task (Tab. 3).

Tabulka 3: MICs between EEG-fMRI SPMs over different frequency bands and classic heuristic model for visual oddball task: all 30 electrodes of interest; On diagonal, there are entropies of given SPMs. Except the diagonal, values higher than 0.75 are highlighted in bold [28].

δ	θ	α	β	γ	HM	
4.28	0.49	**1.10**	0.48	0.48	0.70	δ
	4.26	0.70	0.33	0.38	0.64	θ
		4.56	0.43	0.43	0.65	α
			3.88	0.45	0.51	β
				4.32	**0.98**	γ
					4.45	HM

3.10 Conclusion

The conclusions are predominantly declared based on visuall oddball data results, since the semantic decision data results were possibly damaged by the eye-blinking artifact.

The visual oddball data results show that the absolute and relative EEG powers are indicators of different brain processes, and that they are associated differently with fMRI data. From that point of view transformation between absolute and relative EEG power fluctuations can be considered as non-linear operation. While the absolute power showed dominantly a broad spectrum component in task-unrelated networks, the relative power showed activity in the visual, sensory-motor, and motor networks. Simultaneously it has been showed that relative power describes the task-related activity better than absolute power and that it is able to suppress the broad spectrum component. From this point of view, it has been shown that relative EEG power appears to be a better indicator of task-related activations for joint EEG-fMRI analysis [29].

Matrices of mutual informations between EEG-fMRI SPMs of different heuristic models has similar structure over both tested datasets. Classic heuristic model visualized similar EEG-fMRI SPMs which are observed with generalized spectral heuristic model for γ frequency band. More on visual oddball data, the generalized spectral heuristic model demonstrated task-related visual network for α band pattern, which were not observable with the classic heuristic model. From that point of view, generalized spectral heuristic model was able to see more task-related networks and should be preferred because of that before the classic model, since the γ band pattern is able to see similar activations as the classic model.

The current analyses and experiments brought two main novelties into the current state of the art. Relative EEG power could be more usable in task-related networks visualizations from simultaneous EEG-fMRI data. And, generalized spectral heuristic model could visualize more task-related networks than the classic model.

4 EEG-fMRI spatiospectral heuristic model

4.1 Visual oddball and semantic decision datasets

Same EEG-fMRI datasets with same acquisition parameters was used as described within previous *subchapters 3.1 "Visual oddball task and EEG-fMRI acquisition"* and *3.2 "Semantic decision task and EEG-fMRI acquisition"*

4.2 Resting-state paradigm and EEG-fMRI acquisition

Fifty healthy subjects participated in a 15 min "resting-state" experiment (30 right handed men, 20 right-handed women; age 25 ± 5 years). Subjects were instructed to lie still within the fMRI scanner with their eyes closed, not to think of anything specific, and not to fall asleep.

The imaging was performed by a 1.5 T *Siemens Symphony* scanner equipped with *Numaris 4 System (MRease)*. High-resolution anatomical T1-weighted MPRAGE images were acquired (160 sagittal slices, matrix size 256 x 256 resampled to 512 x 512, slice thickness = 1.17mm, TR = 1700ms, TE = 3.96ms, FOV = 246mm, FA = 15°).

Functional images were acquired using gradient echo, echo-planar imaging sequence: TR = 3000 ms; TE = 40 ms; FOV = 220 × 220 mm; FA = 90°; matrix size 64 × 64 (3.9 × 3.9 mm); slice thickness = 3.5 mm; and 32 transversal slices which covered the whole brain excluding part of the cerebellum. 300 functional scans were acquired in 1 continuous session.

Simultaneously, scalp EEG data were recorded with a 30-electrode MR compatible EEG system (*BrainProducts, Germany*). ECG were recorded to remove physiological artifacts from EEG. Signals were sampled at 5 kHz with 0.5μV resolution for EEG, and 10μV for ECG.

4.3 EEG and fMRI data preprocessing

The preprocessing steps were the same as in previous *sub-chapter 3.3 "EEG and fMRI data preprocessing"*. The eye-blinking artifact was not removed from resting-state EEG dataset, since the subjects had closed eyes.

4.4 EEG spatiospectral decomposition

For each session, the preprocessed EEG signal from each lead was normalized such that the time course was normally distributed $N(0,1)$, and divided into 1.66 s (the shortest repetition time of fMRI scanning TR) epochs without overlap. Each epoch was transformed to the spectral domain with fast Fourier transform (FFT), generating a vector (length = 67) of complex valued spectral coefficients between 0-40Hz. Complex values were converted to absolute/relative power. The output vector of 67 real absolute/relative power values comprised a 3D matrix $\boldsymbol{E}$ with dimensions n_t , n_c and

n_ω. Dimension n_T is the total number of EEG epochs ($n_T = 540$ for RST; $n_T = 255$ for SDT; $n_T = 256$ for VOT), dimension n_c is the total number of leads ($n_c = 30$) and dimension n_ω is the total number of spectral coefficients ($n_\omega = 67$). The 3D matrix $\boldsymbol{E}(n_T, n_c, n_\omega)$ was transformed into a 2D matrix $\boldsymbol{E}(n_T, n_c * n_\omega)$. Matrix $\boldsymbol{D}$ is estimated with two-stage PCA from $\boldsymbol{E}$ matrices of all subjects and used as input into group spatiospectral ICA decomposition (eq. 7) [8], returning a group aggregated mixing matrix $\hat{\boldsymbol{A}}$ with dimensions $\hat{\boldsymbol{A}}(n_T, m)$ and a group aggregated source matrix $\hat{\boldsymbol{S}}$ with dimensions $\hat{\boldsymbol{S}}(m, n_c * n_\omega)$. The dimension m is the number of set and decomposed independent components [27].

$$\boldsymbol{D} = \boldsymbol{H} = \hat{\boldsymbol{A}}\hat{\boldsymbol{S}} \tag{7}$$

The first stage PCA reduced dimensionality of single-subject matrices $\boldsymbol{E}$ at 50 dimensions from original 540 dimensions for RST, 255 for SDT and 256 for VOT. The second stage PCA reduced the group variability at 20 principal components. Group spatiospectral ICA was conducted separately for each paradigm and power type, and the data were decomposed to $m = 20$ independent spatiospectral components. The PCA data reduction and whole group ICA decomposition were performed using the GIFT toolbox [10] with the INFOMAX optimizing algorithm [7]. The reproducibility of group components was examined using 10 ICASSO itterations when the cluster quality index evaluated the cluster's stability [17].

The analysis outputs are group-derived aggregated matrices $\hat{\boldsymbol{A}}$ and $\hat{\boldsymbol{A}}$ for each paradigm and separate $\boldsymbol{A}$ and $\boldsymbol{S}$ matrices generated by back reconstruction against each individual subject's data. The spatiospectral matrices $\boldsymbol{S}$ were collected across subjects and paradigms for clustering (separately for each power type), as described below. The relationship between spatiospectral components/sources and task dynamics were examined by relating the source time course (i.e. mixing matrix) $\boldsymbol{A}$ with the respective stimulus time course [27].

4.5 Clustering of spatiospectral maps across paradigms

For each subject, paradigm and session (4 sessions for VOT data), we have one matrix $\boldsymbol{S}$ with dimensions $\boldsymbol{S}(20, 2010)$ containing 20 back-reconstructed spatiospectral patterns. For similarity/dissimilarity assessment of the spatiospectral patterns across paradigms, we have performed k-means clustering, a conventional algorithm belonging to multivariate methods for dimensionality reduction. Because we had 50 single-subject $\boldsymbol{S}$ matrices for "rest", 42 single-subject $\boldsymbol{S}$ matrices for semantic decision task and 21×4 = 84 single-subject $\boldsymbol{S}$ matrices for visual oddball task, there are $(50 + 42 + 84) * 20 = 3520$ different spatiospectral patterns comprising matrix $\boldsymbol{C}$, with dimensions $\boldsymbol{C}(3520, 2010)$ for input into k-means clustering. K-means clustering was performed with Pascual-Marqui et al. (1995) optimizing method [38] with set 40 final clusters.

Clustering was repeated 50 times with random initial conditions and the result with minimal residuals was selected as the final clustering result [27].

4.6 Spatiospectral pattern dynamics and stimuli vectors

For each subject, paradigm and session, we have got one matrix $\boldsymbol{A}$ with dimensions $\boldsymbol{A}(n_T, 20)$ containing the back-reconstructed time course of each spatiospectral component. Relationships between these dynamics and stimulus vector timings were assessed with a single-subject general linear model and a continuous group one-sample t-test for the each stimulus vector as we have implemented previously [29, 27].

4.7 EEG-fMRI GLM with variable HRFs

Relationships between fMRI voxel time courses and spatiospectral map time courses (columns in individual $\boldsymbol{A}$ matrices) were examined using the GLM with the individual time course convolved with the canonical HRF (regressor 1), convolved with the 1^{st} temporal derivative of the HRF (regressor 2) or convolved with the 2^{nd} temporal derivative of the HRF (regressor 3) as in [35]. Using the canonical HRF and 1^{st} and 2^{nd} temporal derivatives helps account for variability in the IRF's shape across subjects, tasks, and voxels.

Separate GLMs were performed for each stable spatiospectral pattern, paradigm and subject. In addition to the three EEG regressors, the model matrix contained a DC component. Regression matrices were estimated over all GLMs with the ReML algorithm (Restricted Maximum Likelihood) implemented in SPM12 software (*Wellcome Trust Centre for Neuroimaging, London, UK*) in the MATLAB programming environment (*MathWorks, Natick, USA*).

Group-averaged EEG-fMRI results were estimated with a one-way ANOVA test (implemented in SPM12) of 3 EEG-derived single-subject spatial regression-maps for each of 3 EEG regressors. The regression-map weights served as dependent variables in separate ANOVA tests conducted for each paradigm and spatiospectral pattern (i.e. 3 paradigms * 14 stable spatiospectral patterns = 42 tests), generating group-averaged spatial EEG-fMRI F-maps.

4.8 Results

Visual inspection among the spatiospectral maps generated across paradigms suggests that similar components may be observed across all three datasets [27]. Similar visual observations you may find also among the relative EEG power components. Since we have visually observed similar group-averaged spatiospectral patterns, we have designed single-subject k-means clustering of the patterns and tested whether some patterns are really stable over datasets.

The k-means clustering was performed separately for each power type with same algorithm settings. For each power type, the original 3520 dimensions (i.e. 3520 spatiospectral patterns) were reduced to 40 representative cluster centroids. Forty output clusters were selected after examining the compactness. The simplified result visualization is shown in Fig. 3, where representative spatiospectral map is demonstrated for each cluster and radial dendrogram projection is included. K-means clustering analysis indicates that similar EEG spatiospectral patterns appear across different tasks. Fifteen clusters (cl. numbers 2, 4, 5, 9, $\{13; 3\}$, 16, $\{17; 27\}$, $\{18; 20\}$, 30, 32, 37, 39) define 12 different spatiospectral patterns which are observable in all tasks, with more than 89% of subjects from each dataset present within each cluster. In general, these spatiospectral maps appear consistent with maps generated in previous studies [8, 7] and appear biologically plausible, demonstrating power within characteristic EEG frequency bands [27].

Two spatiospectral patterns which are observable in all datasets were divided at six disjunctive clusters where each cluster belongs to one specific dataset. The radial dendrogram projection (Fig. 3), these clusters form 2 different but neighbouring groups and each group corresponds to an unique spatiospectral pattern (cl. numbers $\{6; 29; 38\}$ and $\{19; 22; 33\}$). As demonstrated, 21 of 30 clusters characterize 14 different spatiospectral patterns which are observable and relatively stable in all three datasets. For exceptions, we note that clusters 25 and 31 contain some spatiospectral patterns which are present only during task, while the patterns of clusters 10 and 15 were present only during "rest" [27].

For the relative EEG power, we have got following k-means clustering results. Twenty-one of the 40 output clusters were organized into 16 final K-means clusters (Fig. 4) whose spatiospectral patterns appear to be of physiological origin. Thirteen clusters were not included since their patterns consisted of single-frequency peak which appeared artefactual, and which was not present over the 3 paradigms. The remaining 6 excluded clusters contained less than 5% of single-subject patterns of at least one paradigm and are thus considered noise. Twelve of the sixteen patterns derived from relative EEG power were stable over all three paradigms (Fig. 4a,b). Of these twelve stable sources, ten appeared visually similar to patterns that were observed for absolute EEG power (Fig. 4a). Two stable γ-band patterns (Fig. 4b) were present with relative power but not with absolute power. One cluster representing β-band activity ($\sim$20Hz) was present for SDT and VOT data but not RST (Fig. 4c). Three clusters contained maps (one θ-band and two γ-band patterns) which were present during RST but not SDT or VOT (Fig. 4d) [26].

The t-values of relationships between EEG spatiospectral pattern time-courses $\boldsymbol{A}$ and stimulus vectors are listed in Table 4. The critical t-values rejecting the null hypothesis, that there is no evidence between compared signals, is 2.1 for $p<0.05$ uncorrected, 3.0 for $p<0.05$ corrected (FWE correction) and 3.22 for $p<0.001$ uncorrected for multiple comparisons. Although significant relationships with stimulus vectors were

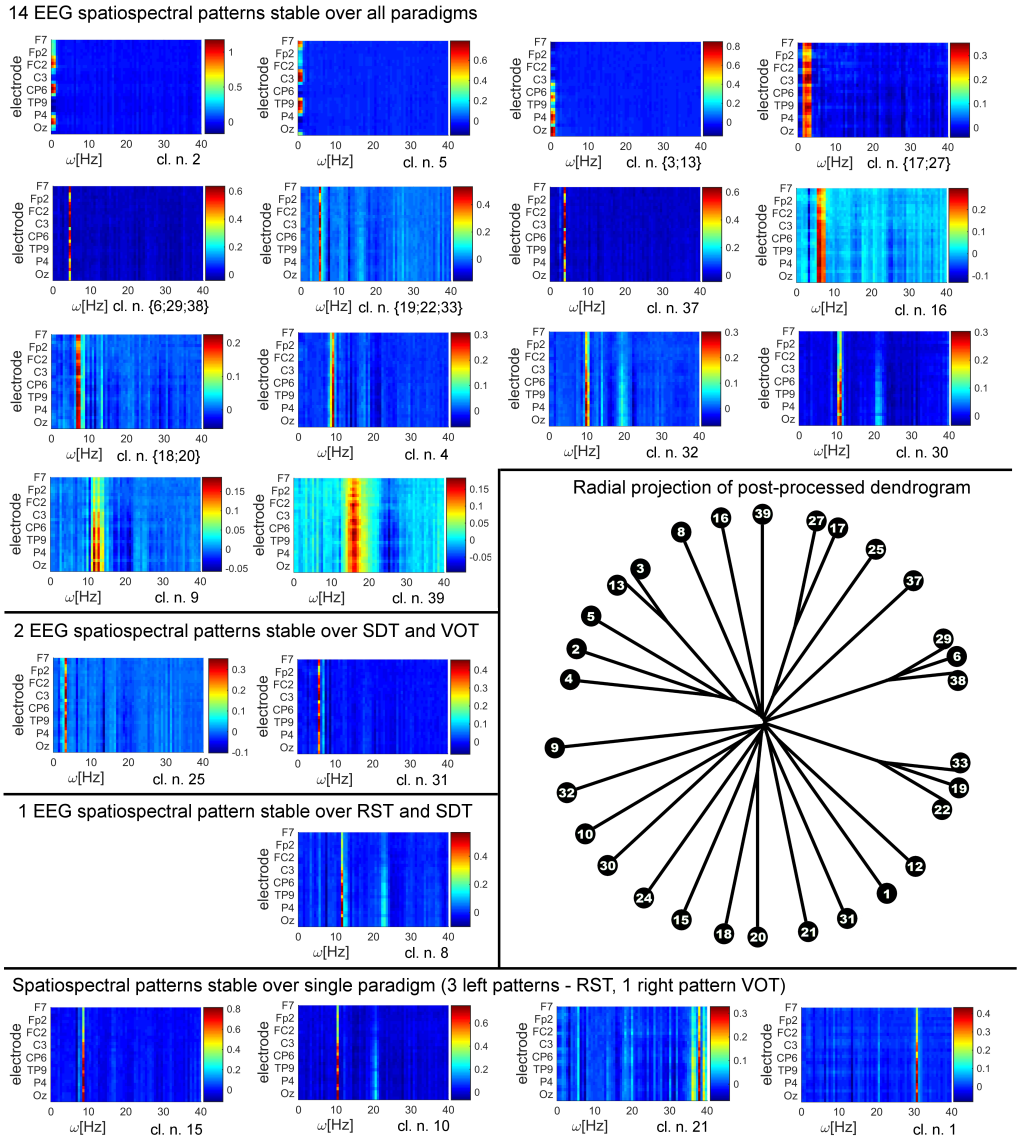

Obrázek 3: Simplified absolute EEG power k-means clustering result visualization over all tested paradigms [27].

found for both power types, there appears to be no statistically significant difference in the distribution of |t|-values computed between power types. The difference between absolute or relative power relationships with the stimuli is $p < 0.162$ based on two-sample t-test between distributions or $p < 0.150$ based on a 10 000 sample bootstrap test [26]. The most of the tests did not reach statistical significance using conservative corrections for multiple comparisons. And probably, it is more true for the absolute EEG power than for the relative EEG power, where we observe some supra-threshold values after the correction.

We have made some observations suggesting that relative power overcomes the absolute power again. Since the table of relationships between EEG spatiospectral pattern timecourses and stimulus vectors demonstrate higher relationships for the relative power (Table 4) and since several spatiospectral patterns appear to be stable for both

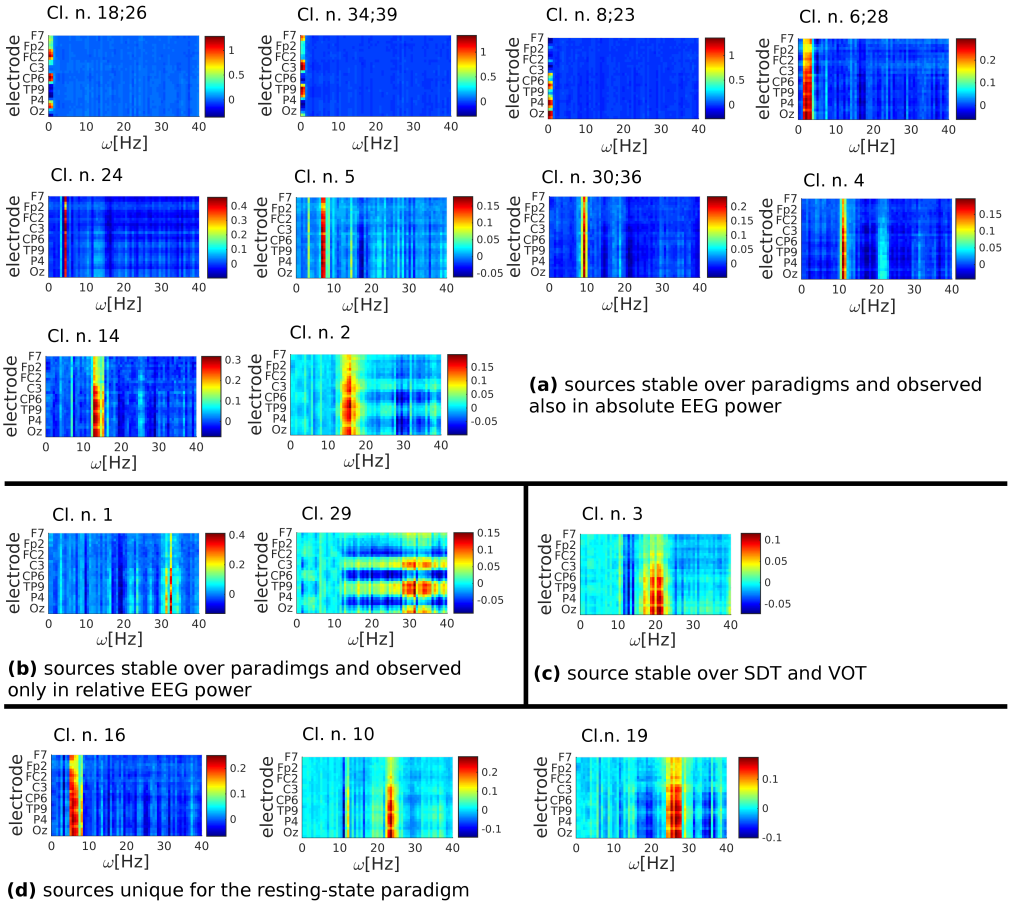

Obrázek 4: Relative EEG power k-means clustering result visualization [26].

Tabulka 4: Relationships between timecourses A and stimulus vectors: The black bold highlighted values are t-values with $p < 0.05$ uncorrected. The green bold highlighted values are t-values with $p_{FWE} < 0.05$.

Absolute power					Relative power				
Cl. n.	frequent	target	distractor	sentences	Cl. n.	frequent	target	distractor	sentences
2	-1.13	0.43	-0.52	0.93	1	-0.58	-1.86	0.21	0.08
5	-0.81	1.77	0.31	-0.63	2	**-3.74**	-1.40	-1.31	-0.05
3;13	-1.45	**2.43**	0.21	-0.09	4	0.12	0.21	0.40	**-2.88**
17;27	-2.09	0.24	**-2.24**	-	5	-0.13	1.14	-1.50	0.76
19;38;6	-0.34	**2.37**	-0.25	-1.63	14	**-3.28**	-1.44	-0.97	0.26
22;33;19	-0.27	-0.23	-0.97	-0.25	24	-2.03	**2.17**	0.01	0.24
37	-1.13	-0.40	0.56	-0.73	29	-0.08	0.57	0.47	0.33
16	**-2.47**	1.20	-0.83	-0.72	8;23	-1.45	**2.46**	-0.35	0.01
18;20	0.39	0.39	-1.00	-1.45	34;39	-0.92	**2.63**	1.30	-0.86
4	1.72	**2.62**	0.56	-0.86	18;26	-1.01	1.45	-0.43	1.00
32	1.67	0.73	0.12	-1.10	6;28	**-4.32**	1.04	-1.46	-0.29
30	**2.48**	0.58	-0.34	-1.87	30;36	**2.59**	1.82	1.65	-1.67
9	**-3.23**	-0.52	-0.61	0.21	3	2.06	-0.86	-1.86	0.27
39	-0.17	-0.06	-0.61	0.21					

power types (Figs. 3 and 4), we have compared EEG-fMRI results for the pattern appearing for both power types with the highest evidence to the stimulus vectors (Fig. 5). On the first view, it could seems that both powers visualize the same large scale brain

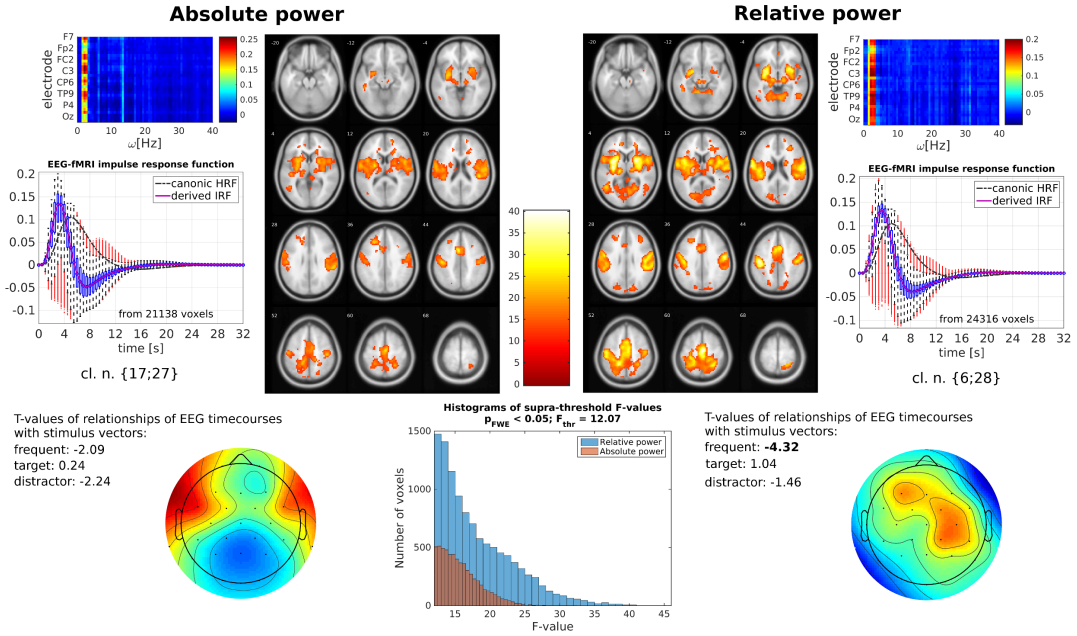

Obrázek 5: Absolute versus relative EEG-fMRI results for the low θ-band spatiospectral pattern with the highest evidence to the task: VOT task, both EEG-fMRI maps threshold at $p_{FWE} < 0.05$, the colorbar between F-maps is the same for both F-maps.

network involving sensory-motor cortices and basal ganglia working together. But relative power results are statistically stronger over almost all observations. The F-values are higher, the supra-threshold areas are larger (or the amount of supra-threshold voxels is higher), the evidence to the frequent stimulus is higher and supra-threshold after correction for multiple comparisons. The estimated impulse response functions between EEG and fMRI signals appear to be almost the same.

Other three clusters (cl. n. $\{34; 39\}$, $\{8; 23\}$ and 24; Fig. 4) dispose with significant relationship to the target stimulus with p<0.05 uncorrected for multiple comparison errors (Table 4). Clusters n. $\{34; 39\}$ and $\{8; 23\}$ did not show any significant EEG-fMRI correlates at significance level $p_{FWE} < 0.05$. Oppositely, the cluster n. 24 demonstrate significant EEG-fMRI associations at significance level $p_{FWE} < 0.05$ in left-side lateralized sensory-motor networks (i.e. contralateral to right handed pushed button) and in left Putamen (Fig. 6).

Timecourses of the spatiospectral pattern of cluster n. 4 are significantly related to the sentence stimulus during the semantic decision task (Table 4 and Fig. 4). Although we have reported that our SDT EEG data are distorted with eye-blinking artifact and that it possibly decreases the strength of EEG-fMRI couplings, we are observing deactivations in Wenricke's areas (part of the speech cortex reliable for the speech understanding) after the α-band pattern (cl. n. 4) increase (Fig. 7). As you can see on the scalp topology, the decrease in α-band corresponds with Wenricke's area location. we have not noticed with any other approach suprathreshold EEG-fMRI relationships in stimulated speech areas.

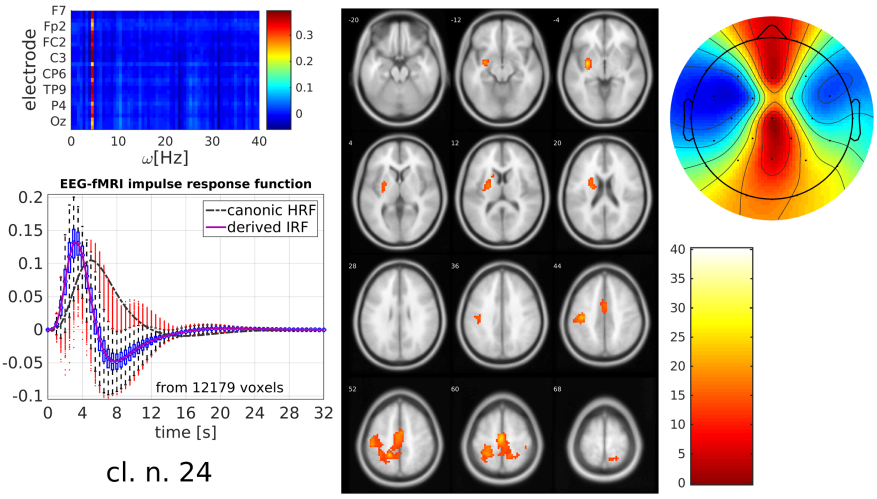

Obrázek 6: EEG-fMRI results for the θ-band spatiospectral pattern related to the target stimulus: VOT task, EEG-fMRI F-map threshold at $p_{FWE} < 0.05$.

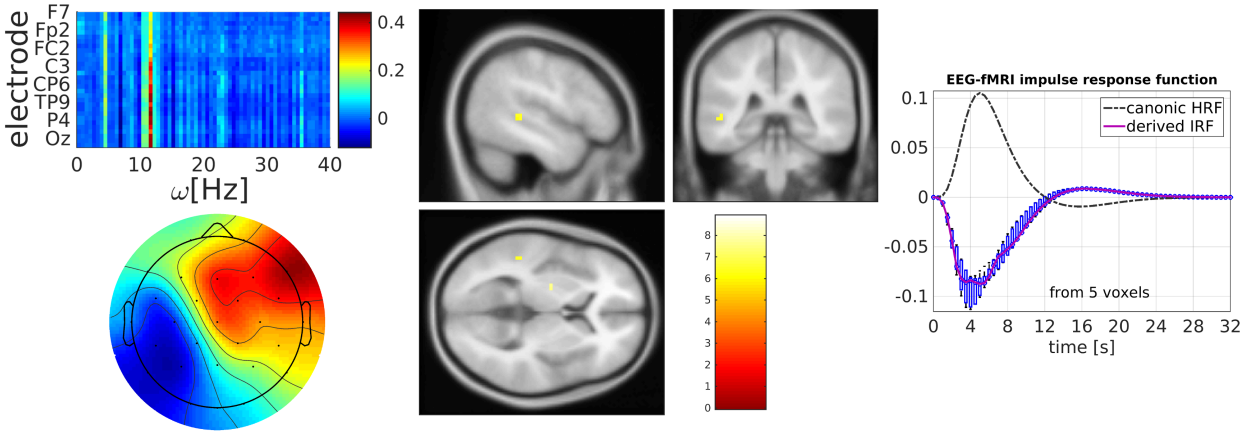

Obrázek 7: EEG-fMRI results for the α-band spatiospectral pattern related to the semantic blocked sentence stimulus: SDT task, EEG-fMRI F-map threshold at $p < 0.001$ uncorrected for multiple comparison errors.

4.9 Novelty in EEG decomposition and following EEG-fMRI fusion

To the best of our knowledge and knowledge of other scientists [19], the present doctoral thesis and publications related to the thesis are the first to demonstrate the stability of EEG independent spatiospectral patterns over different datasets. These findings further validate the approach for future studies, and motivate investigation of the functional role of the distinct spatiospectral patterns. Subdividing spectral responses in a data driven manner will be useful for future studies that decompose separate signals with potentially distinct functional roles (i.e. generating more robust results) and separating signals from artifact (i.e. enhancing signal over noise) [27].

This is the first study examining EEG-fMRI correlates after group-derived EEG spatiospectral decomposition over different experimental datasets. The voxel-wise EEG-fMRI approach revealed F-statistic fMRI overlays whose supra-threshold voxels

organized into functional large scale brain networks (LSBNs) consistent with previous literature. In addition, we have modelled spatially variable group-averaged HRFs often with shorter latency peaks than the canonical HRF.

We have designed the generalized EEG-fMRI spatiospectral heuristic model and proposed how to solve the model with the spatiospectral group-ICA method [28]. Since the model demonstrates the most significant task-related EEG-fMRI associations over the range of tested approaches (i.e. absolute power fluctuations, generalized spectral heuristic model, fluctuations of absolute power spatiospectral patterns), its application can be expected in future research of blind visualizations of task-related networks directly from simultaneous EEG-fMRI data. Obtained statistical significance of EEG-fMRI results for the VOT task-related networks is one of the highest which can be observed over literature nowadays.

The knowledge, that relative EEG power spatiospectral patterns are stable over different paradigms [26] is also novel and unique.

4.10 Conclusion

As the first in the world, we have shown and published that spatiospectral group-ICA of EEG spectra estimates stable independent spatiospectral patterns over datasets and possibly also over subjects. That applies for both power types (i.e. absolute and relative powers). Obtained higher statistical significance for EEG-fMRI results with EEG spatiospectral F-maps proves that better incorporation of the channels together with modelled spatially and timely variable hemodynamic response improved the method of the data fusion. Our designed generalized spatiospectral heuristic model dispose with the highest evidence in task-related network visualizations and it possibly will become to be used in future simultaneous EEG-fMRI data fusion research. The inter-subject variability of significant obtained results were not investigated within the current thesis and it should be done within the near future research.

5 Doctoral thesis outcomes and conclusions

We have set seven partial goals necessary for the successful defense of the current doctoral thesis (see 2^{nd} *chapter "Doctoral thesis objectives"*).

Ad. 1.: Because the goal was to visualize task-related brain networks without information about the stimulus timings inside the EEG-fMRI fusion, we have selected the EEG processing via power spectral changes instead of the event related potentials, where timings of the trial beginnings are necessary.

Ad. 2.: The literature review uncovered that the most of EEG-fMRI data fusion processes use absolute EEG power fluctuations which are compared with delayed fMRI-BOLD signals. The usage of the relative EEG power fluctuations in distinct frequency bands were not commonly used, although Klimesch 1999 and Kilner et

al. (2005) [23, 24] claim it corresponds more with evoked neuronal activity. Kilner et al. (2005) proposed and Rosa et al. (2010) simplified the classic heuristic approach (eq. 4) [23, 41] which expects same global changes over whole relative power frequency range after evoked neural activity, although e.g. inhibition hypothesis was tested and confirmed for the α-band pattern [25] (i.e. it behaves antagonistic to the other frequency bands). To overcome this limit, we have designed generalized spectral heuristic model (eq. 5), which we are testing within the current doctoral thesis. The generalized spectral heuristic model has still limit in utilizing unique informations from different EEG leads, as evaluated in 3^{rd} chapter of the current thesis. To overcome this issue, we have proposed generalized spatiospectral heuristic model (eq. 6) and designed how to solve it with spatiospectral group-ICA. Since the group-ICA belongs to the family of blind source separation algorithms and stability of its estimates over different runs/datasets/etc. is still speculative, we have used existing k-means clustering algorithm and estimated the stability of the EEG spatiospectral sources over different datasets and subjects. Following EEG-fMRI associations were then evaluated and tested only for the stable spatiospectral patterns. For the EEG-fMRI data fusion, general linear model was used for both proposed and tested models. The BOLD signal delay in EEG power fluctuations was modelled as fixed canonical hemodynamic response function for the generalized spectral heuristic model, and as spatially and temporally variable hemodynamic response function for the generalized spatiospectral heuristic model.

Ad. 3.: To evaluate the correspondence with external stimulation, general linear model between EEG power fluctuations and stimulus vectors was implemented with following group one-sample t-tests. The stimulus vectors were regressors and EEG power fluctuations were the measured data.

Ad. 4.: We have implemented the EEG-fMRI fusion for the original absolute power fluctuations, classic heuristic model, generalized spectral heuristic model, time-courses of stable absolute power spatiospectral patterns and stable patterns of generalized spatiospectral heuristic model. Simultaneous EEG-fMRI data were acquired for visual oddball, semantic decision and resting-state experiments, and were more or less used for the evaluation of differences over different fusion approaches.

Ad. 5.: It was shown that both proposed models (i.e. generalized spectral and spatiospectral heuristic models) visualize task-related networks from EEG-fMRI data better than previous available approaches. The spectral model did not ignore the α-band inhibition properties of the EEG signal. And the spatiospectral model utilized better the information about different sources over different leads. The spatiospectral heuristic model disposed with highest statistical significance of the task-related results for visual oddball data. For semantic decision data, it was the only one approach which was able to show supra-threshold activated voxels in speech areas, although the semantic decision EEG data were distorted with eye-blinking artifact. Beyond the original objectives, we have found that EEG absolute and relative power spatiospectral

patterns are stable over different paradigms and subjects, and that the stability is much higher than other concurrent actually used ICA decompositions of EEG signal.

Ad. 6.: First, we have presented in *Journal of Neuroscience Methods* that relative EEG power in distinct frequency bands (i.e. the generalized spectral heuristic model) is better for visualizations of task-related brain networks than originally commonly used absolute power [29]. Then we have proposed generalized spectral and spatiospectral heuristic models with a preliminary results on 13^{th} *International Symposium on Biomedical Imaging: From Nano to Macro* [28]. During the testing of the spatiospectral group-ICA as the method for EEG signal processing into the form comparable with BOLD signals, we have noticed that the estimates are stable and similar over different paradigms for both power types (i.e. absolute and relative). For the absolute power, we have reported this acquired knowledge in *Brain Topography* journal within the special issue *Multisubject Decomposition of EEG — Methods and Applications* [27]. For the relative power, we have submitted the obtained results as conference proceedings on *World Congress on Medical Physics & Biomedical Engineering* [26]. The proceedings is under review now. The EEG-fMRI results for the stable absolute power spatiospectral sources are summarized within prepared manuscript *"EEG spatiospectral patterns and their link to fMRI BOLD signal via variable hemodynamic response functions"* which will be submitted into a journal in several following weeks. Since we have got the most significant EEG-fMRI task-related networks for the generalized spatiospectral heuristic model, we are expecting that this result could be written as an other manuscript and submitted to a journal. Except these published or prepared or planned papers related to the current doctoral thesis, I was helpful during testing the stability of EEG-fMRI fusion after EEG signal PARAFAC decomposition (parallel factor analysis). The PARAFAC results were presented in *Neural Computation* journal [34].

Ad. 7.: The list of attached functions is given within appendix *B* of the full-length Doctoral Thesis.

6 Abstract

Lots of different data fusion strategies have been developed during last 15 years of simultaneous EEG-fMRI research. The current doctoral thesis summarizes the actual state of the art in EEG-fMRI data fusion research and puts a goal to improve task-related network visualizations blindly directly from the acquired data. Two different models which should improve it have been proposed within the thesis (i.e. generalized spectral heuristic model and generalized spatiospectral heuristic model). Generalized spectral heuristic model utilizes relative EEG power fluctuations in distinct frequency bands averaged over electrodes of interest and compares the fluctuations with delayed BOLD signal fluctuations via general liner model. The obtained results shows that the model visualizes several different frequency dependent task-related EEG-fMRI networks. The model overcomes the absolute power fluctuation approach and classic heuristic approach too. The absolute power visualized a task-not-related broadband EEG-fMRI component and classic heuristic model was insensitive to visualize the task-related visual network which was observed for the relative α-band pattern for visual oddball task data. For the semantic decision task EEG-fMRI data, the frequency dependence was not so evident in final results. Since all the bands visualized only visual network and any areas of speech network, the results were possibly corrupted by not-suppressed eye-blinking artifact in EEG data. Mutual information coefficients between different EEG-fMRI statistical parametric maps showed that the similarities over different frequency bands are similar over different tasks (i.e. visual oddball and semantic decision). More, the coefficients proved that averaging over different electrodes of interest does not bring any new information into the joint analysis, i.e. the signal on one single lead is very smoothed signal from the whole scalp. For that reasons, better incorporation of the channel information into the EEG-fMRI analysis started to be necessary and we have proposed more general spatiospectral heuristic model and designed how to estimate the model with spatiospectral Group Independent Component Analysis of EEG spectra relative power. The obtained results show that spatiospectral heuristic model visualizes the statistically most significant task-related networks (compared to absolute power spatiospectral pattern results and generalized spectral heuristic model results). The spatiospectral heuristic model was the only one, which observed task-related activations in a speech areas for semantic decision data. Beyond the fusion of EEG spatiospectral patterns with fMRI data, we have tested the stability of the spatiospectral pattern estimates over different paradigms (i.e. visual oddball, semantic decision and resting-state) with k-means clustering algorithm. We have got 14 stable patterns for the absolute EEG power and 12 stable patterns for the relative EEG power. Although ten of the patterns appear similar over the power types, the relative power spatiospectral patterns (i.e. spatiospectral heuristic model patterns) have higher evidence to tasks.

Reference

[1] P J ALLEN, O JOSEPHS, and R TURNER. *A method for removing imaging artifact from continuous EEG recorded during functional MRI.* NeuroImage, 12(2):230–9, aug 2000.

[2] P J ALLEN, G POLIZZI, K KRAKOW, D R FISH, and L LEMIEUX. *Identification of EEG events in the MR scanner: the problem of pulse artifact and a method for its subtraction.* NeuroImage, 8(3):229–239, 1998.

[3] Christian-G BÉNAR, Daniele SCHÖN, Stephan GRIMAULT, Bruno NAZARIAN, Boris BURLE, Muriel ROTH, Jean-Michel BADIER, Patrick MARQUIS, Catherine LIEGEOIS-CHAUVEL, and Jean-Luc ANTON. *Single-trial analysis of oddball event-related potentials in simultaneous EEG-fMRI.* Human brain mapping, 28(7):602–613, 2007.

[4] F BLOCH. *Nuclear induction.* Physical Review, 70(7-8):460–474, 1946.

[5] Milan BRÁZDIL, Michal MIKL, Radek MAREČEK, Petr KRUPA, and Ivan REKTOR. *Effective connectivity in target stimulus processing: a dynamic causal modeling study of visual oddball task.* NeuroImage, 35(2):827–835, 2007.

[6] David A. BRIDWELL and Vince CALHOUN. *Fusing Concurrent EEG and fMRI intrinsic networks.* In Magnetoencephalography, pages 213–235. Springer, Berlin Heidelberg, 2014.

[7] David A. BRIDWELL, Srinivas RACHAKONDA, Rogers F. SILVA, Godfrey D. PEARLSON, and Vince D. CALHOUN. *Spatiospectral Decomposition of Multisubject EEG: Evaluating Blind Source Separation Algorithms on Real and Realistic Simulated Data.* Brain Topography, 31(1):47–61, 2018.

[8] David A BRIDWELL, Lei WU, Tom EICHELE, and Vince D CALHOUN. *The spatiospectral characterization of brain networks: fusing concurrent EEG spectra and fMRI maps.* NeuroImage, 69:101–11, apr 2013.

[9] Gregory BUZSAKI. *Rhythms of the Brain.* Oxford University Press, 2006.

[10] V D CALHOUN, T ADALI, G D PEARLSON, and J J PEKAR. *A Method for Making Group Inferences from Functional MRI Data Using Independent Component Analysis.* Human brain mapping, 14:140–151, 2001.

[11] Pierre COMON. *Independent component analysis, A new concept?* Signal Processing, 36(3):287–314, apr 1994.

[12] J C DE MUNCK, S I GONcCALVES, R MAMMOLITI, R M HEETHAAR, and F H LOPES DA SILVA. *Interactions between different EEG frequency bands and their effect on alpha-fMRI correlations.* NeuroImage, 47(1):69–76, aug 2009.

[13] K J FRISTON, J ASHBURNER, C D FRITH, J POLINE, J D HEATHER, and R S J FRACKOWIAK. *Spatial Registration and Normalization of Images*. *Human brain mapping*, 3(3):165–189, 1995.

[14] A. GARTUS, T. FOKI, A. GEISSLER, and Roland BEISTEINER. *Improvement of clinical language localization with an overt semantic and syntactic language functional MR imaging paradigm*. *American Journal of Neuroradiology*, 30(10):1977–1985, 2009.

[15] Robin I. GOLDMAN, John M. STERN, Jerome ENGEL, and Mark S. COHEN. *Acquiring simultaneous EEG and functional MRI*. *Clinical Neurophysiology*, 111(11):1974–1980, 2000.

[16] Robin I GOLDMAN, John M. STERN, Jerome Jr ENGEL, and Mark S. COHEN. *Simultaneous EEG and fMRI of alpha rhythm*. *Neuroreport*, 13(18):2487–2492, 2002.

[17] Johan HIMBERG, Aapo HYVÄRINEN, and Fabrizio ESPOSITO. *Validating the independent components of neuroimaging time series via clustering and visualization*. *NeuroImage*, 22(3):1214–1222, 2004.

[18] Frank R. HUANG-HELLINGER, Hans C. BREITER, Glen MCCORMACK, Mark S. COHEN, Ken K. KWONG, Jeffrey P. SUTTON, Robert L. SAVOY, Robert M. WEISSKOFF, Timothly L. DAVIS, John R. BAKER, John W. BELLIVEAU, and Bruce R. ROSEN. *Simultaneous functional magnetic resonance imaging and electrophysiological recording*. *Human Brain Mapping*, 3(1):13–23, 1995.

[19] R.J. HUSTER and V.D. CALHOUN. *Progress in EEG: Multi-subject Decomposition and Other Advanced Signal Processing Approaches*. *Brain Topography*, 31(1):1–2, 2018.

[20] Aapo HYVÄRINEN, Pavan RAMKUMAR, Lauri PARKKONEN, and Riitta HARI. *Independent component analysis of short-time Fourier transforms for spontaneous EEG/MEG analysis*. *NeuroImage*, 49(1):257–271, 2010.

[21] Jiří JAN. *Medical Image Processing, Reconstruction and Restoration: concepts and methods*. Taylor & Francis Group, Boca Raton, 2006.

[22] Tzyy-ping JUNG, Scott MAKEIG, Colin HUMPHRIES, Te-Won LEE, Martin J. MCKEOWN, Vicente IRAGUI, and Terrence J. SEJNOWSKI. *Removing electroencephalographic artifacts by blind source separation*. *Psychophysiology*, 37(2):S0048577200980259, 2000.

[23] J.M. M KILNER, J. MATTOUT, R. HENSON, and K.J. J FRISTON. *Hemodynamic correlates of EEG: a heuristic.* *NeuroImage*, 28(1):280–286, oct 2005.

[24] W KLIMESCH. *EEG alpha and theta oscillations reflect cognitive and memory performance: a review and analysis.* Brain research reviews, 29(2-3):169–95, apr 1999.

[25] Wolfgang KLIMESCH, Paul SAUSENG, and Simon HANSLMAYR. *EEG alpha oscillations: the inhibition-timing hypothesis.* Brain research reviews, 53(1):63–88, jan 2007.

[26] René LABOUNEK, David A. BRIDWELL, Radek MAREČEK, Martin LAMOŠ, Michal MIKL, Milan BRÁZDIL, Jiří JAN, and Petr HLUŠTÍK. *Stable EEG spatiospectral sources using relative power as group-ICA input*. In World Congress on Medical Physics & Biomedical engineering [Under Review], 2018.

[27] René LABOUNEK, David A BRIDWELL, Radek MAREČEK, Martin LAMOŠ, Michal MIKL, Tomáš SLAVÍČEK, Petr BEDNAŘÍK, Jaromír BAŠTINEC, Petr HLUŠTÍK, Milan BRÁZDIL, and Jiří JAN. *Stable scalp EEG spatiospectral patterns across paradigms estimated by group ICA*. Brain Topography, 31(1):76–89, 2018.

[28] René LABOUNEK, David JANEČEK, Radek MAREČEK, Martin LAMOŠ, Tomáš SLAVÍČEK, Michal MIKL, Jaromír BAŠTINEC, Petr BEDNAŘÍK, David BRIDWELL, Milan BRÁZDIL, and Jiří JAN. *Generalized EEG-fMRI spectral and spatiospectral heuristic models*. In 13th International Symposium on Biomedical Imaging: From Nano to Macro, pages 767–770, Prague, 2016. IEEE.

[29] René LABOUNEK, Martin LAMOŠ, Radek MAREČEK, Milan BRÁZDIL, and Jiří JAN. *Exploring task-related variability in fMRI data using fluctuations in power spectrum of simultaneously acquired EEG*. Journal of Neuroscience Methods, 245:125–136, 2015.

[30] René LABOUNEK, Martin LAMOŠ, Radek MAREČEK, and Jiří JAN. *Analysis of connections between simultaneous EEG and fMRI data*. In 19th International Conference on Systems, Signals and Image Processing, number April, pages 576–579, Vienna, Austria, 2012.

[31] H LAUFS, A KLEINSCHMIDT, A BEYERLE, E EGER, A SALEK-HADDADI, C PREIBISCH, and K KRAKOW. *EEG-correlated fMRI of human alpha activity*. NeuroImage, 19(4):1463–1476, aug 2003.

[32] P. C. LAUTERBUR. *Image Formation by Induced Local Interactions: Examples Employing Nuclear Magnetic Resonance*. Nature, 242:190–191, 1973.

[33] D MANTINI, M G PERRUCCI, C DEL GRATTA, G L ROMANI, and M CORBETTA. *Electrophysiological signatures of resting state networks in the human brain.* Proceedings of the National Academy of Sciences of the United States of America, 104(32):13170–5, aug 2007.

[34] Radek MAREČEK, Martin LAMOŠ, René LABOUNEK, Marek BARTOŇ, Tomáš SLAVÍČEK, Michal MIKL, Ivan REKTOR, and Milan BRÁZDIL. *Multiway array decomposition of EEG spectrum: Implications of its stability for the exploration of large-scale brain networks*. Neural computation, 29(4), 2017.

[35] Radek MAREČEK, Martin LAMOŠ, Michal MIKL, Marek BARTOŇ, J FAJKUS, Ivan REKTOR, and Milan BRÁZDIL. *What can be found in scalp EEG spectrum beyond common frequency bands. EEG–fMRI study*. Journal of Neural Engineering, 13(4):1–13, 2016.

[36] Kai J MILLER. *Broadband spectral change: evidence for a macroscale correlate of population firing rate?* The Journal of Neuroscience, 30(19):6477–9, may 2010.

[37] S OGAWA, T M LEE, a R KAY, and D W TANK. *Brain magnetic resonance imaging with contrast dependent on blood oxygenation.* In Proceedings of the National Academy of Sciences of the United States of America, volume 87, pages 9868–72, dec 1990.

[38] R.D. PASCUAL-MARQUI, C.M. MICHEL, and D. LEHMANN. *Low resolution electromagnetic tomography: a new method for localizing electrical activity in the brain*. International Journal of Psychophysiology, 18(1):49–65, 1994.

[39] E M PURCELL. *Spontaneous Emission Probabilities at Radio Frequencies*. In Proceedings of the American Physical Society, volume 69, page 681, 1946.

[40] I. I. RABI. *Space Quantization in a Gyrating Magnetic Field*. Physical Review, 51(1):652–654, 1937.

[41] M J ROSA, J KILNER, F BLANKENBURG, O JOSEPHS, and W PENNY. *Estimating the transfer function from neuronal activity to BOLD using simultaneous EEG-fMRI.* NeuroImage, 49(2):1496–509, jan 2010.

[42] René SCHEERINGA, M. C M BASTIAANSEN, Karl Magnus PETERSSON, Robert OOSTENVELD, David G. NORRIS, and Peter HAGOORT. *Frontal theta EEG activity correlates negatively with the default mode network in resting state*. International Journal of Psychophysiology, 67(3):242–251, 2008.

[43] S VULLIEMOZ, R RODIONOV, D W CARMICHAEL, R THORNTON, M GUYE, S D LHATOO, C M MICHEL, J S DUNCAN, and L LEMIEUX. *Continuous EEG source imaging enhances analysis of EEG-fMRI in focal epilepsy.* NeuroImage, 49(4):3219–29, feb 2010.